THE JOURNAL OF PHYSICAL CHEMISTRY C
A JOURNAL OF THE AMERICAN CHEMICAL SOCIETY

pubs.acs.org/JPCC

Article

Understanding Quantum Plasmonic Enhancement in Nanorod Dimers from Time-Dependent Orbital-Free Density Functional Theory

Hongping Xiang,* Jiaxing Zu, Hongwei Jiang, Lin Xu,* Gang Lu, and Xu Zhang*

Cite This: *J. Phys. Chem. C* 2022, 126, 5046−5054

Read Online

ACCESS | Metrics & More | Article Recommendations

ABSTRACT: Localized surface plasmon resonances could yield extreme enhancement of local electric fields at surfaces of plasmonic nanostructures. Herein, we have performed quantum mechanical simulations to systematically study plasmonic resonances in sodium (Na) nanorod dimers based on time-dependent orbital-free density functional theory. Several representative geometries, including end-to-end, side-to-side, and right-angle T- and L-shaped dimer arrangements are explored in detail. The optical spectra, tunneling electric current, and electric field enhancement (hot spots) are examined as a function of the size of the nanorods, their relative arrangement, and their gap distance (≤2 nm). Two plasmon resonant modes are identified to be responsible for the observed electric field enhancement. One of them is of quantum nature, arising from quantum tunneling across the gap of the two nanorods. The other mode is of electrostatic nature, originating from the dipolar interaction between the plasmonic oscillations of each nanorod. Among the examined geometries, the end-to-end dimer exhibits the strongest field enhancement, which increases with the aspect ratio and the gap distance. The interplay between electron tunneling across the gap and the spill-out of electrons at the nanorod surfaces is revealed to dominate the modulation of plasmonic resonances and field enhancement in the nanorod dimers.

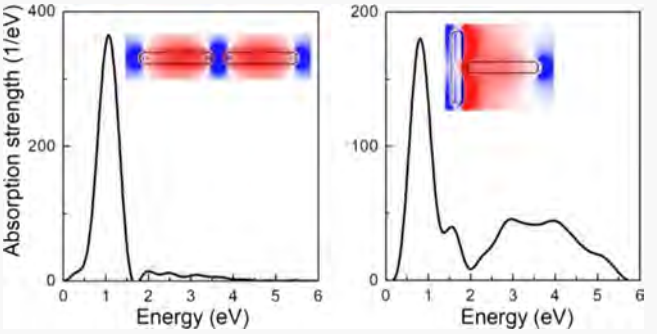

1. INTRODUCTION

Metallic nanorods are attractive plasmonic nanostructures thanks to their anisotropic shapes that could yield both longitudinal and transverse modes of localized surface plasmon resonances (LSPRs), with electron oscillations along the axial and radial directions, respectively, upon electromagnetic radiation.[1−8] The LSPRs depend on the chemical composition and geometry (e.g., radius, length, and aspect ratio) of the nanorods. More importantly, they can also be tuned through near-field couplings between adjacent nanorods.[9−13] The interaction between the LSPR modes in the coupled nanorods could produce great enhancement in local electric fields,[14−17] which is responsible for phenomena such as surface-enhanced Raman scattering,[16−19] fluorescence,[20−23] second harmonic generation,[24] and two-photon photoluminescence.[25] As a result, the coupled nanorods are promising components for various plasmonic applications, ranging from sensing,[26] biomedical technologies,[27,28] and metamaterials,[29] to nanoscale light polarizers,[30] and optoelectronic devices.[31,32]

The simplest coupled nanorods are dimers in which two rods are separated by a small gap (about a few nanometers). Despite the simplicity, the dimer could host a myriad of intriguing phenomena[33−36] and some of which will be examined below. A fertile playground in the field is to explore the geometric dependence of plasmonic resonances. For example, an interesting geometry is an end-to-end arrangement in which the coupled LSPRs are in the visible region and can be tuned in an ultrasensitive manner in optical detection systems.[33,37−39] Indeed, significant research effort in past decades has been devoted to coupled nanorods, in terms of both experimental demonstrations of various phenomena and their theoretical understanding.

To the best of our knowledge, most experimental and theoretical studies so far have focused on nanorod dimers with the dimensions over 20 nm and the gap distance above 2 nm.[36,40−44] When the dimension of nanorods becomes less than 10 nm and the gap distance is less than 2 nm, the quantum effects ranging from electron density spill-out to electron tunneling play an important role in the LSPRs which

Received: January 6, 2022
Revised: February 17, 2022
Published: March 2, 2022

https://doi.org/10.1021/acs.jpcc.2c00105
J. Phys. Chem. C 2022, 126, 5046−5054

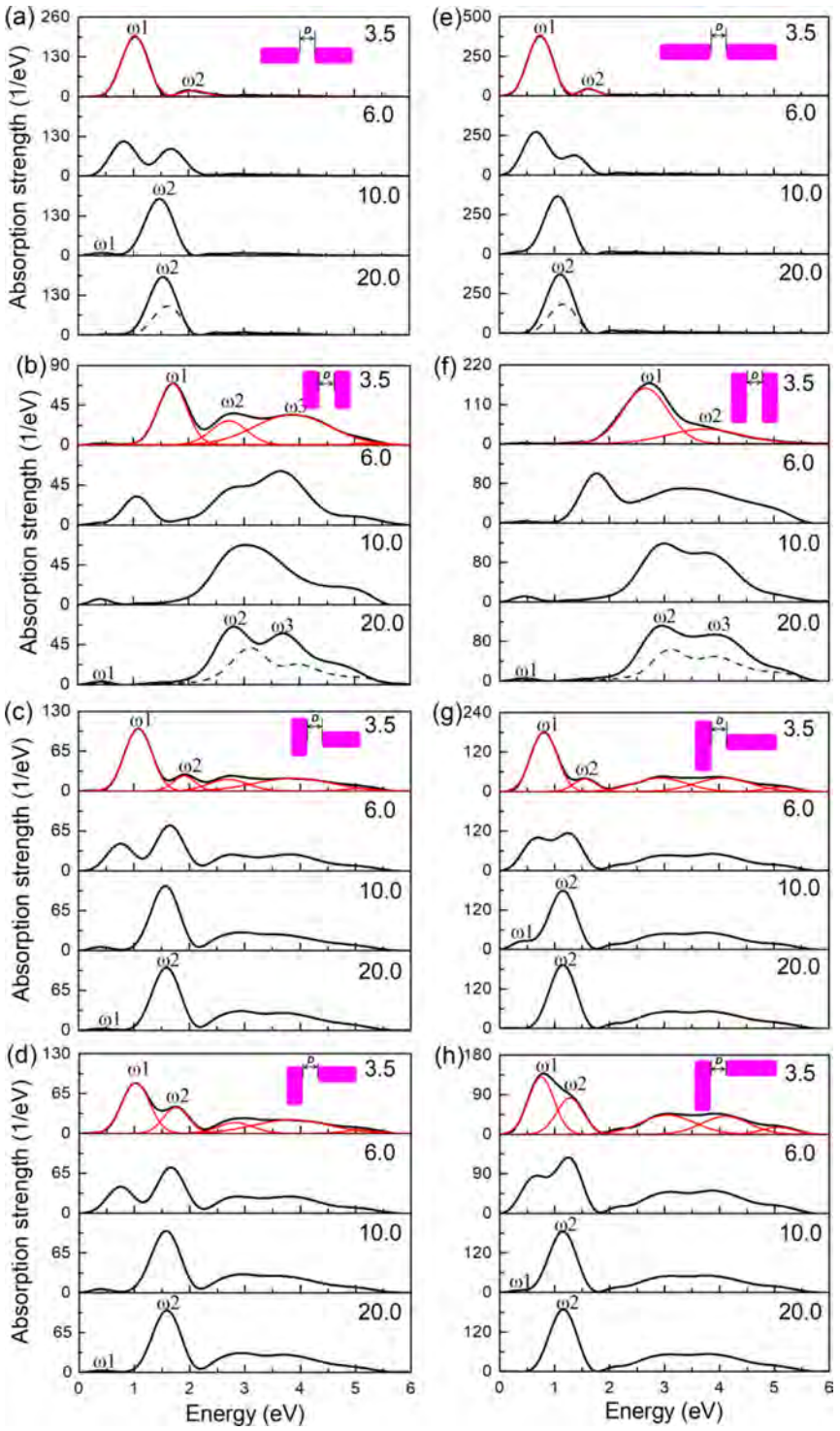

Figure 1. Optical absorption spectra of Na nanorod dimers with the aspect ratio l/d of the individual rod of 3.5 (l = 30 Å, d = 8.6 Å, N_{atom} = 67) (a–d) and 6.5 (l = 55.9 Å, d = 8.6 Å, N_{atom} = 126) (e–h) in the end-to-end, side-to-side, T-shaped, and L-shaped geometries (inserted in purple), as a function of the gap distance D. Black dashed curves are the optical spectra of a single nanorod. Resolved Gaussian spectra are shown in red.

yield novel optoelectronic properties.[45−48] However, the experimental fabrication of such smaller nanorods and dimers at short distances apart remains a challenge. The theoretical research on nanorod dimers is mainly realized by solving the Maxwell equations of classical theory through numerical methods,[33,35,43,49−51] which cannot capture the quantum effects.

Here, we investigate the quantum plasmonics in nanorod homodimers based on a recently developed time-dependent orbital-free density functional theory (TD-OFDFT)[52] which shows comparable accuracy to that of time-dependent Kohn–Sham density functional theory and was successfully employed to examine the quantum plasmonics in coupled Na nanosphere dimers and trimers[53] as well as single nanorods.[54] In particular, we study the quantum plasmonic coupling between longi-

https://doi.org/10.1021/acs.jpcc.2c00105
J. Phys. Chem. C 2022, 126, 5046−5054

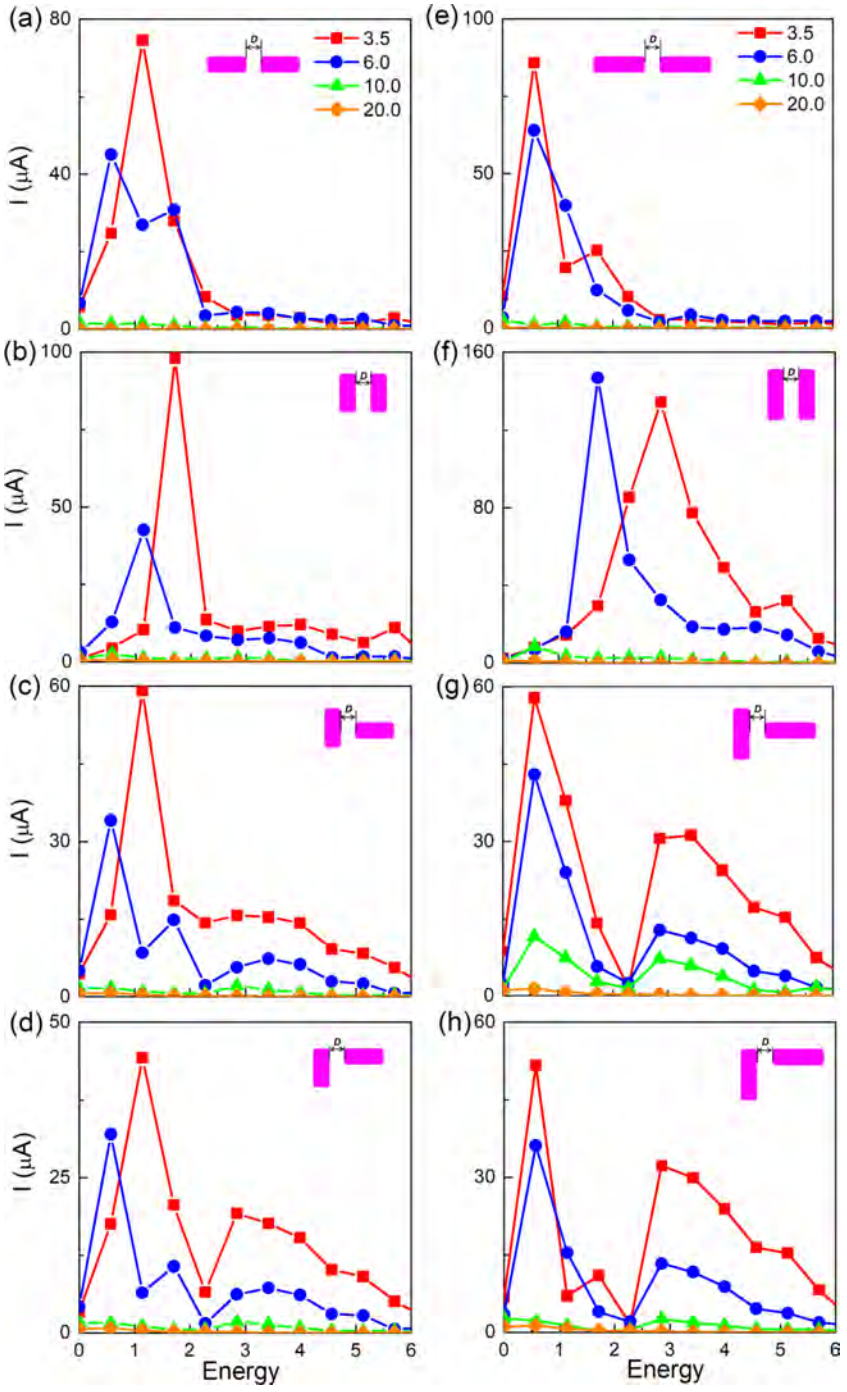

Figure 2. Current density I (μA) across the gap as a function of the plasmon energy for the gap distance of D = 3.5, 6.0, 10, and 20 Å, of the dimers with the individual rods of (a–d) l/d = 3.5 (l = 30 Å, d = 8.6 Å, N_{atom} = 67) and of (e–f) l/d = 6.5 (l = 55.9 Å, d = 8.6 Å, N_{atom} = 126) in the end-to-end, side-to-side, T- and L-shaped geometries (inserted in purple).

tudinal modes and transverse modes by constructing the end-to-end, side-to-side, and right-angle L- and T-shaped nanorod homodimers with the dimension of a few nanometers. Two sizes of nanorods with the aspect ratios l/d of 3.5 and 6.5 are chosen in which the spectra of longitudinal and transverse modes are fully separated and can be individually characterized, with the gap distance set in the subnanometer (<2 nm). We find that the electronic spill-out and tunneling effect tuned by the size of the nanorod, arrangement of the dimer, and gap distance, has a great influence on the optical absorption spectra and local electric field enhancement.

2. METHODOLOGY AND STRUCTURE MODELS

In the TD-OFDFT calculations, the charge density was propagated in a real-space grid in real-time under the influence of time-varying electric fields with an interparticle axial direction of the dimer. The local density approximation was used for the electron exchange and correlation in both the ground state and excited state calculations.[55] The ionic potential of Na was described by a local pseudopotential calculated based on the first-principles theory.[52,56] To eliminate particle–particle interactions, a convergence check on the size of the supercell has been performed and it is found

https://doi.org/10.1021/acs.jpcc.2c00105
J. Phys. Chem. C 2022, 126, 5046–5054

that the dimension of the supercell with 2.5 times the length of the Na nanorod dimer is sufficient. The Na nanorod dimmer was placed at the center of the supercell. A uniform mesh grid with a spacing of 0.35 Å, which has been verified to yield a converged result,[52,57] was employed over which the charge density and potential were calculated. The simulation zone beyond which the charge density vanishes was defined by assigning a sphere with a radius of 8 Å around each atom, which is necessary for achieving numerical convergence. Fast Fourier transform was employed to efficiently calculate the convolution integrals in the kinetic energy functional and the Coulomb potential. The linear response calculations were performed by propagating the electron wave packets under a perturbation of an impulse field $E(t) = E_{kick}\delta(t)$.[58] The electronic wave packets in the real-time propagation were evolved for 7500 steps with a time step of $\Delta t = 0.0015\ \hbar/\text{eV}$.

The structure models of nanorods were built from a face-centered cubic Na supercell, which can be described as a quasicylinder by its full-length l, and diameter d, with the aspect ratio defined as l/d. All the nanorods have the same shape and density with the shortest distance between Na atoms of 2.491 Å. Here, we consider two sizes of sodium nanorods, a smaller one with the aspect ratio l/d of 3.5 (l = 30 Å, d = 8.6 Å, N_{atom} = 67), and a larger one with l/d of 6.5 (l = 55.9 Å, d = 8.6 Å, N_{atom} = 126). Both rods have fully separated spectra of longitudinal and transverse modes and thus can be individually characterized.[54] In addition, the rod of l/d = 6.5 has a larger spill-out effect induced by the larger aspect ratio.[54] Four kinds of configuration homodimers were constructed: end-to-end (Figure 1a,e), side-to-side (Figure 1b,f), and right-angle T- (Figure 1c,g) and L-shaped (Figure 1d,h) geometries. Several gap distances D of the dimer were considered including 20.0, 10.0, 6.0, and 3.5 Å. We calculate the absorption spectra, tunneling current at the gap, and local electric field enhancement (hot spots) of all constructed structural models with the polarization direction along with the interparticle axis (a horizontal polarization). The time-dependent electric current across the gap was Fourier transformed to yield the frequency-dependent electric current.

3. RESULTS AND DISCUSSION

Figure 1 displays the optical absorption spectra as a function of the gap distance D. As a reference, the longitudinal and transversal plasmonic spectra of the single nanorod are shown in Figure 1a,b, respectively. The frequency-dependent electric current passing across the gap is shown in Figure 2. We resolve each absorption spectrum as a sum of Gaussian functions and derive several distinctive resonance modes such as the main peaks termed ω1, ω2, and ω3 in Figure 1 (red curves). It can be seen that the sum of the Gaussians matches very well the original absorption spectrum for each model. Figures 3456 present the induced charge densities (relative to the equilibrium values) and the corresponding electric field distributions at the main absorption frequencies (ω1 and ω2 in Figure 1) of all structural models, respectively, which were obtained by Fourier transform of the charge density and electric field distribution from the time domain to the frequency domain.

3.1. Rods Aligned End-to-End. The hybridization theory predicts two plasmon coupling modes in the end-to-end dimer: the bonding plasmon mode with a lower energy and the antibonding plasmon mode with a higher energy.[59−61] In the homodimer, the bonding plasmon mode (BDP) between the longitudinal modes is bright, while the anti-BDP is dark due to zero net dipole.[33,36] The anti-BDP can be only observed as a bright one in an asymmetric heterodimer. As the gap distance of the dimer is reduced, the bonding longitudinal mode shows a significant redshift and an increase of the effective polarizability relative to the single nanorod,[62] and the near-field enhancement at the gap becomes greater.[33,62,63]

The BDP mode is revealed in the end-to-end nanorod dimer, e.g., the aspect ratio of l/d = 3.5 and gap distance D of 20.0 Å. As shown in Figure 1a, the absorption spectra are dominated by an extremely intense peak labeled ω2, which is red-shifted compared to the longitudinal plasmon mode of the individual rod (black dash line in Figure 1a). This absorption peak is attributed to the BDP mode, which originates from the hybridization between the longitudinal dipolar plasmon modes of the individual nanorods. The redshift relative to single nanorod stems from the electrostatic attractive interaction of longitudinal plasmon modes of the individual rods, which has been observed in the large-size (a few tens of nanometers) nanorod dimers[33,62] and the nanosphere dimers.[53]

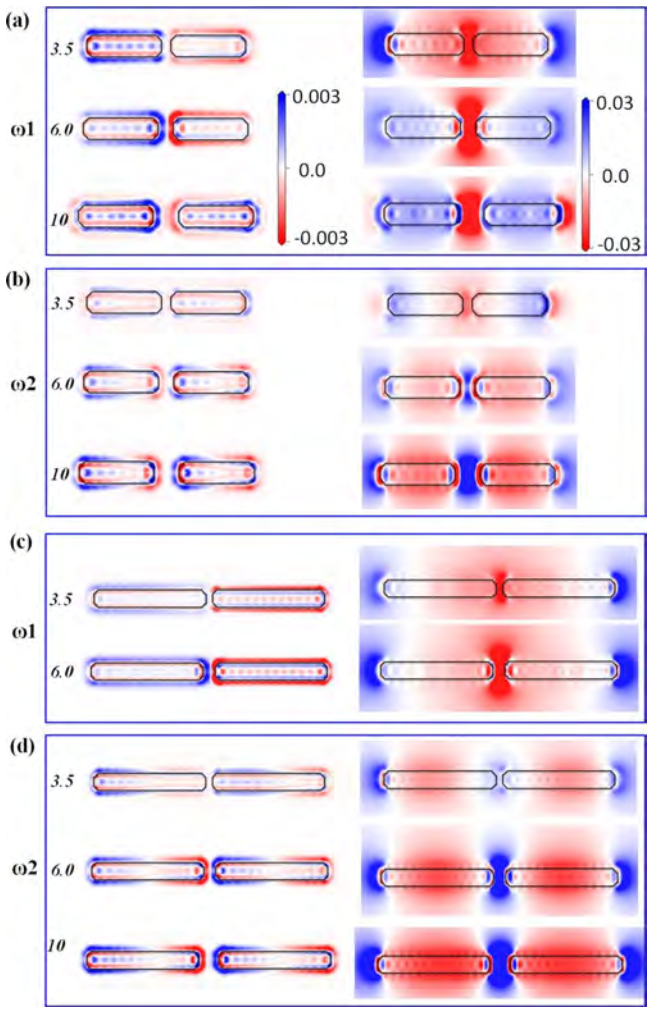

Figure 3. Induced charge density (atomic unit) (left panel of each figure) and electrical field (atomic unit) (right panel of each figure) evaluated at the frequency ω1 and ω2 as shown in Figure 1a,e in response to a horizontal polarization (along interparticle axis), for the dimer of l/d = 3.5 (a,b) and 6.5 (c,d) in the end-to-end geometry. Magnitude of the charge density is color-coded in (a).

https://doi.org/10.1021/acs.jpcc.2c00105
J. Phys. Chem. C 2022, 126, 5046−5054

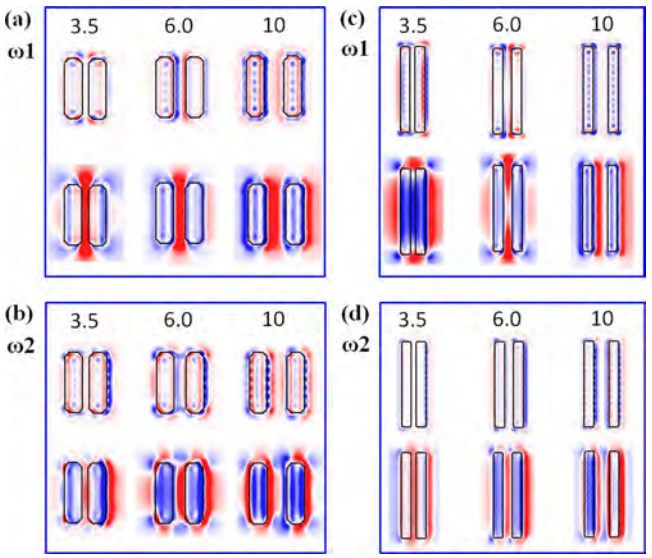

Figure 4. Induced charge density (atomic unit) (upper panel of each figure) and electrical field (atomic unit) (lower panel of each figure) evaluated at the frequency $\omega 1$ and $\omega 2$ as shown in Figure 1b,f in response to a horizontal polarization (along interparticle axis), for the dimer of l/d = 3.5 (a,b) and 6.5 (c,d) in the side-to-side geometry. Magnitude of the charge density is color-coded in Figure 3a.

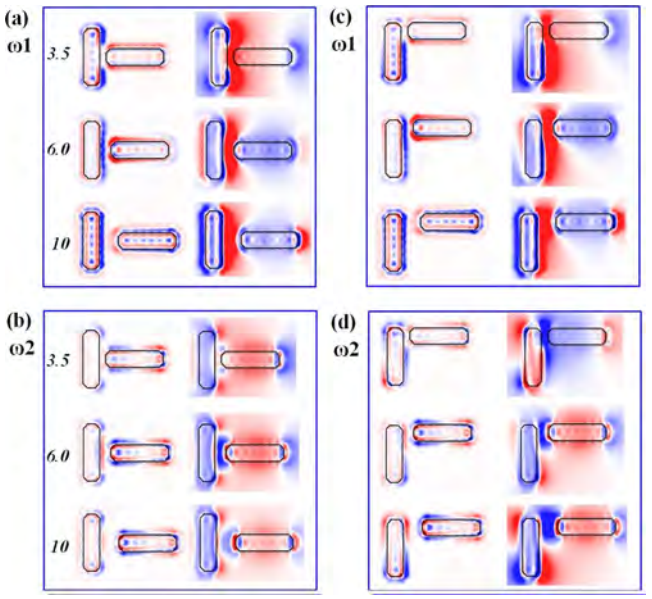

Figure 5. Induced charge density (atomic unit) (left panel of each figure) and electrical field (atomic unit) (right panel of each figure) evaluated at the frequency $\omega 1$ and $\omega 2$ as shown in Figure 1c,d in response to a horizontal polarization (along interparticle axis), for the dimer of l/d = 3.5 in the T- (a,b) and L-shaped (c,d) geometries. Magnitude of the charge density is color-coded in Figure 3a.

When D is reduced to 10 Å, electron tunneling takes place resulting in charge transfer between nanorods. Thus, a new charge transfer plasmon (CTP1, $\omega 1$) forms in the lower energy region, and the origin BDP transits to the charge transfer plasmon (CTP2, $\omega 2$) as shown in Figure 1a. CTP2 ($\omega 2$) corresponds to the plasmonic oscillations on the individual rods modified by the charge transfer, while CTP1 ($\omega 1$) is attributed to the tunneled electrons oscillating between the two rods. As D is further reduced to 6.0 Å, CTP1 ($\omega 1$) blue

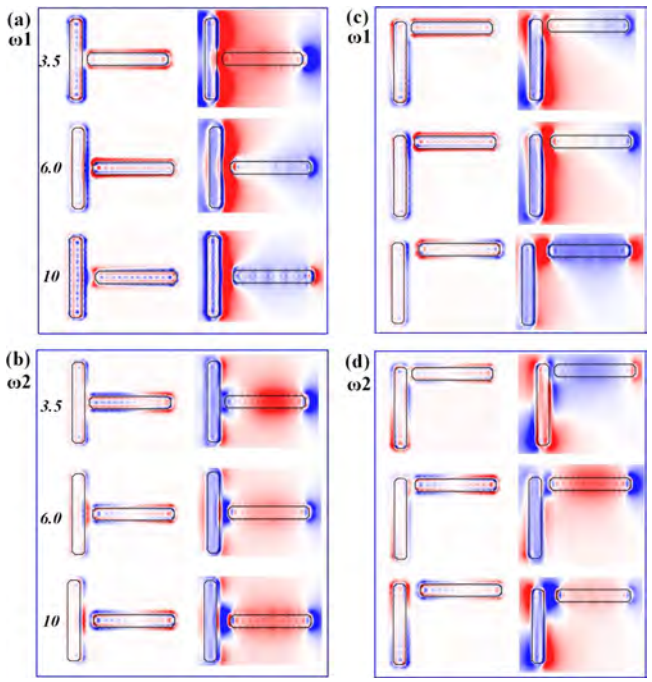

Figure 6. Induced charge density (atomic unit) (left panel of each figure) and electrical field (atomic unit) (right panel of each figure) evaluated at the frequency $\omega 1$ and $\omega 2$ as shown in Figure 1g,h in response to a horizontal polarization (along interparticle axis), for the dimer of l/d = 6.5 in the T- (a,b) and L-shaped (c,d) geometries. Magnitude of the charge density is color-coded in Figure 3a.

shifts with the intensity increasing strongly. On the contrary, the intensity of CTP2 ($\omega 2$) which is proportional to the number of conduction electrons on each rod, decreases rapidly, even lower than that of CTP1. It indicates that more conduction electrons involved in CTP2 transform to tunneling electrons involved in CTP1 by reducing the gap. This can be verified from the results of electron current across the gap as shown in Figure 2a. An appreciable tunneling current is observed as D reduces to 6 Å, with peaks at both CTP1 and CTP2 as expected. Similar to the nanosphere dimer,[53] as the two rods approach each other, their electrostatic interaction energy increases while the average electron excitation energy decreases. The latter dominates the former as D reduces from 10 to 6 Å, thus the resonant energy of CTP2 ($\omega 2$) is blue-shifted.

As D reaches 3.5 Å, the electronic wave functions from the two nanorods start to overlap and a chemical bond may be formed between the outmost atoms of the two nanorods. Thus a conductive channel is established, allowing electron flow across the gap. It is reflected in the extremely strong peak intensity and large tunneling current of CTP1 ($\omega 1$) and an almost disappeared CTP2 ($\omega 2$) as shown in Figures 1a and 2a.

As shown in Figure 3a,b, at D = 10 Å, the charge density of the dimer at CTP2 ($\omega 2$) shows the characteristics of longitudinal dipole plasmon of the single nanorod.[54] The plasmonic oscillations of the two nanorods have the same phase. However, the charge density of CTP1 ($\omega 1$) deviates significantly from that of the single nanorod and displays a typical charge transfer plasmon oscillation in the polarization direction. The electric field distribution at $\omega 1$ shows that the field is enhanced as D decreases from 10 to 6 Å, consistent with the fact that CTP1 originates from the charge transfer across the gap. Then the electron field starts to decrease as D

https://doi.org/10.1021/acs.jpcc.2c00105
J. Phys. Chem. C 2022, 126, 5046−5054

reduces to 3.5 Å because a conductive channel is formed and electrons can flow through the gap, neutralizing the induced charges at the opposite sides of the gap (Figure 3a). By contrast, the electric field is weakened at the gap for $\omega 2$ as D decreases from 10 to 3.5 Å. The comparable field distribution is found at the ends of the dimer for $\omega 2$ at D = 10 Å, which is similar to the field distribution of a single nanorod and reflects the fact that CTP2 results from the plasmon on the individual nanorod.

It can be seen from Figures 1e, 2e and 3c,d, that the nanorod dimer with the aspect ratio of l/d = 6.5 in the end-to-end geometry shows some similarities in terms of the absorption spectra, tunneling current, and local electric field enhancement as a function of the gap distance D to that of the dimer of l/d = 3.5. The striking difference is that at the same gap distance, the charge transfer in the dimer of l/d = 6.5 is much stronger than that in the dimer l/d = 3.5. For example, at D = 6.0 Å, the absorption spectral intensity of CTP1 ($\omega 1$) is much larger than that of CTP2 ($\omega 2$), accompanying a large current across the gap which is almost close to that at D = 3.5 Å (Figure 2e). As a result, the electric field enhancement at the gap for CTP1 ($\omega 1$) at D = 6.0 and 3.5 Å, is weaker than that in the dimer of l/d = 3.5. On the contrary, the electric field at $\omega 2$ distributing at ends and the gap is stronger than that in the dimer of l/d = 3.5. The maximum of the electric field is located at the far end of the single nanorod for the longitudinal dipole mode (CTP2), which becomes stronger as the aspect ratio increases because of a higher volume density of the accumulated electrons.[54]

3.2. Rods Aligned Side-to-Side. For the nanorod dimer with the aspect ratio of l/d = 3.5 in the side-to-side geometry and D = 20.0 Å, a very weak absorption peak ($\omega 1$ in Figure 1b) of CTP1 appears at the lower energy region (around 0.5 eV), implying that the electron tunneling starts to play. This scenario happens at a smaller gap distance of D = 10.0 Å for the dimer in the end-to-end geometry (Figure 1a). According to the LSPRs of the single nanorod (dash line in Figure 1b), the absorption peaks named CTP2 ($\omega 2$) and CTP3 ($\omega 3$) are observed in the higher energy region (>2 eV), which are transited from the bonding dipolar modes and bonding Bennett quadrupole modes.[54] Both the bonding modes originate from the hybridizations between the transverse dipolar plasmon modes and between the transverse Bennett quadrupole plasmon modes of the individual rods, respectively. The enhanced electron spill-out effect accounts for the strong transverse quadrupole plasmon modes.[54] The spill-out effect increases electrostatic interaction between the two rods, resulting in a redshift of CTP2 ($\omega 2$) and CTP3 ($\omega 3$) relative to that of single nanorod is observed as shown in Figure 1b.

As D decreases from 20.0 to 3.5 Å, the positions of CTP2 ($\omega 2$) and CTP3 ($\omega 3$) modes almost keep the same, and the absorption intensity is slightly changed. However, the CTP1 ($\omega 1$), which is formed by the electron tunneling between the two nanorods, exhibits strong blue-shift accompanied with the intensity increasing greatly. It is interesting to find that as D decreases from 20.0 to 6.0 Å, the absorption intensity of CTP1 increases while CTP2 decreases greatly and CTP3 changes little. As D further decreases to 3.5 Å, the absorption intensity of CTP1 further increases, CTP2 changes little while CTP3 decreases greatly. Apparently, at a smaller gap distance, some conduction electrons involved in the quadrupole modes (CTP3, $\omega 3$) transit to tunneling electrons involved in CTP1.

The induced charge densities in Figure 4a,b (left panel) show that CTP1 ($\omega 1$) exhibits a typical charge transfer plasmon oscillation, while CTP2 ($\omega 2$) displays a bonding transverse dipole mode which originates from the hybridization between the transverse dipolar plasmon modes of the individual rods. It can be seen from the corresponding electric field distribution (right panel, Figure 4a) that an electric field enhancement at the gap keeps the same as D reduces from 10 to 3.5 Å for CTP1 ($\omega 1$), indicating that the electrons flowing through the gap do not neutralize the charge induced by the charge transfer at the opposite sides of the gap. The electric field distribution at $\omega 2$ (CTP2) of the dimer at D = 10 Å (right panel, Figure 4b) resembles that of the transverse dipole mode of an individual nanorod.[54] As D decreases to 3.5 Å, a very weak electric field is observed at the gap, indicating a conductive channel in this mode.

The dimer of l/d = 6.5 in the side-to-side geometry shows some similar properties of LSPRs as a function of D, to that in the dimer of l/d = 3.5 (Figure 1f). For example, a weak charge transfer mode ($\omega 1$ in Figure 1f) appears in the lower energy region at D = 20.0 Å, and the absorption peaks of CTP2 and CTP3 show a large redshift compared to that of a single nanorod. However, at D = 6.0 Å, the electron current in the dimer of l/d = 6.5 reaches the maximum (Figure 2f), and a conductive channel is observed in Figure 4c in which the electrons can flow through it. As D decreases to 3.5 Å, the CTP1 ($\omega 1$) greatly blue shifts and merges with the CTP2 ($\omega 2$) as shown in Figure 1f. The charge densities and electric field distributions of CTP2 ($\omega 2$) and CTP3 ($\omega 3$) at D = 3.5 Å in Figure 4c are quite similar to those of the transverse dipole mode and Bennett quadrupole mode of the single nanorod whose aspect ratio can be estimated by $l/d = 55.6/(2 \times 8.6 + 3.5) = 2.68$, respectively. The charge transfer is extremely strong in the dimer with a larger aspect ratio, which makes the rods in the dimer easy to bond as a single rod.

3.3. Rods Arranged in T and L Geometries. For the nanorod dimer with the aspect ratio of l/d = 3.5 in the T- and L-shaped geometries, the CTP1 mode ($\omega 1$ in Figure 1c,d) exists at the energy around 0.5 eV with a very small intensity at D = 20.0 Å. It indicates that the electron tunneling takes place at D = 20.0 Å in both geometries similar to the side-to-side geometry. According to the LSPRs of the single nanorod (black dash line in Figure 1a,b), the strongest absorption peak CTP2 ($\omega 2$ in Figure 1c,d) corresponds to the longitudinal dipole mode of the right-side nanorod of the dimer, while the higher energy absorption peaks (>2 eV) originate from the transverse dipole and quadrupole modes of the left-side nanorod of the dimer. In T- and L-shaped geometries, these transverse plasmon modes almost keep the same in terms of both energy and intensity as D decreases from 20 to 3.5 Å, which is different from the scenario in the side-to-side geometry (Figure 1b). The absorption intensity of $\omega 2$ is weakened and the intensity of $\omega 1$ is strengthened by a reducing gap distance, indicating that more electrons are involved in the charge transfer plasmon from the longitudinal dipole plasmon mode of the right-side nanorod of the dimer.

At D = 6.0 Å, the absorption intensity of $\omega 1$ (CTP1) in the T- and L-shaped dimers is smaller than that of $\omega 2$ (CTP2) (Figure 1c,d), contrary to the situation in the end-to-end dimer with the same gap distance (Figure 1a). In addition, at D = 3.5 Å, the values of electric current of CTP1 ($\omega 1$) are 60 and 48 μA for the T- and L-shaped geometries, respectively, smaller than 78 μA in the end-to-end geometry (Figure 2a) and 100 μA in the side-to-side geometry (Figure 2b). Therefore, the electron tunneling effect and charge transfer are weaker in the

https://doi.org/10.1021/acs.jpcc.2c00105
J. Phys. Chem. C 2022, 126, 5046−5054

T- and L-shaped dimers compared to the end-to-end and side-to-side dimers. The charge transfer in the L-shaped geometry is slightly weaker than that in the T-shaped geometry, reflected by a weaker absorption intensity (Figure 1c,d) and lower current value (Figure 2c,d) at CTP1 (ω1).

The charge density of CTP1 (ω1) of T- and L-shaped dimers (left panel of Figure 5a,c) exhibit a typical charge transfer plasmonic oscillation. An electric field enhancement is observed to distribute over the region surrounding the gap for both geometries (right panel of Figure 5a,c), which becomes stronger as D decreases from 10 to 3.5 Å. As reported for a single nanorod,[54] there is a strong electron spill-out effect in the transverse plasmon mode. The tunneling effect in the CTP1 (ω1) mode enhances the spill-out electrons on the surface of the left rod, resulting in a large symmetric and asymmetric electric field around the gap in the T- and L-shaped geometries, respectively.

The charge density of CTP2 (ω2) in the T-shaped geometry (left panel of Figure 5b) displays a typical coupling between the transverse dipole mode of the left-side rod and the longitudinal dipole mode of the right-side rod. As D decreases from 10 to 6.0 Å, there is a small field enhancement observed for the CTP2 (ω2) mode (Figure 5b), which is more concentrated within the gap compared to the CTP1 (ω1) mode (Figure 5a). However, the field enhancement starts to decrease as D reduces to 3.5 Å, because of the formation of the conductive channel at the gap. For the L-shaped geometry, the charge density of CTP2 (ω2, left panel in Figure 5d) exhibits a coupling between the longitudinal dipole mode of the left-side rod (perpendicular to polarization direction) and the longitudinal dipole mode of the right-side rod (along polarization direction). Here, the CTP2 (ω2) mode is transformed from the bonding dipole mode between the two longitudinal dipolar modes. The electric field not only distributes in the gap of the dimer but also occupies the two sides of the left rod. As D decreases from 10 to 3.5 Å, a little stronger field enhancement is observed at the gap different from that in the T-shaped geometry. This phenomenon has not been observed in the end-to-end and side-by-side geometries (Figures 3b and 4b), and in the nanosphere dimers and trimers.[54]

Figure 1g,h show that the CTP1 mode (ω1) does not appear at D = 20 Å for the dimer with the aspect ratio of l/d = 6.5 in T- and L-shaped geometries, which is different from the scenario that of l/d = 3.5 in the same geometries. As D decreases from 10 to 3.5 Å, the dimer of l/d = 6.5 in T- and L-shaped geometries has similar properties of LSPRs as a function of D to the dimer of l/d = 3.5, e.g., the transverse plasmon modes in the higher energy region (>2 eV) changes little, and electron tunneling only affects CTP1 (ω1) and CTP2 (ω2). As shown in Figure 2g, the peak values of the electric current are 12 and 8 μA in the dimer of l/d = 6.5 in the T-shaped geometry at D = 10.0 Å, which are much larger than that in other configurations with the same gap distance (Figure 2a−d,e,f,h).

The charge density of the dimer of l/d = 6.5 in T- and L-shaped geometries (left panel of Figure 6) displays a similar distribution to that in the dimer of l/d = 3.5, i.e., CTP1 (ω1) exhibits a typical charge transfer plasmon oscillation, while CTP2 (ω2) exhibits a transverse−longitudinal coupling mode in the T-shaped geometry and longitudinal−longitudinal coupling mode in the L-shaped geometry. The electrical field in the CTP1 (ω1) mode in the T-shaped geometry distributes not only surrounding the gap but also at the end of the right-side nanorod (Figure 6a), and it is enhanced as D decreases from 10 to 3.5 Å, stronger than that in the dimer of l/d = 3.5 (Figure 5a). The larger the aspect ratio of the nanorod, the stronger the electron spill-out effect for the transversal plasmon mode.[54] When l/d increases from 3.5 to 6.5, the tunneling effect at the gap of the dimer is strengthened by the spill-out electrons of the left rod, resulting in a large electric field at the end of the right rod. In turn, the tunneling electrons further enhance the electron spill-out effect on the surface of the left rod, resulting in the enhancement of the electric field in the upper and lower regions of the gap. However, in the L-shaped geometry, because of the asymmetric arrangement, the interaction between the electron tunneling and spill-out effect decreases greatly as the aspect ratio increases. As a result, the electric field of the L-shaped geometry is weaker than that of the T-shaped geometry.

3.4. Hot Spots. Based on above results, the electric field enhancement or hot spots sensitively depend on the dimer configuration and gap distance. The hot spots mainly originate from two plasmon resonance modes, CTP1 and CTP2. CTP1 is attributed to the oscillation of tunneling electrons between the two rods within the interparticle gap, while CTP2 originates from the electrostatic attractive interaction between the dipolar plasmon modes of the individual rods of the dimer.

For CTP2, the strongest hot spot occurs in the end-to-end dimer, which decreases as the gap distance decreases, but increases as the aspect ratio increases. Thus, the dimer of l/d = 6.5 in the end-to-end geometry at D = 10 Å has the strongest electric field enhancement which is localized in the gap and nanorod ends. For the CTP1 mode, the strongest hot spots occur in the T-shaped dimer, symmetrically distributing over the region surrounding the gap. This electric field increases as the gap distance decreases, and as the aspect ratio increases, because the electron tunneling effect at the gap of the T-shaped dimer increases the spill-out of electrons on the surface of the left rod. In other configurations, the electric fields at CTP1 modes are not only greatly affected by the aspect ratio, symmetry, and gap distance, but also much weaker and more localized.

4. CONCLUSIONS

We have performed TD-OFDFT calculations to systematically investigate the plasmon resonances, including optical spectra, induced charge density variation, electric current through the gap, and electric filed enhancement, on the sodium nanorod homodimers in the end-to-end, side-to-side, and right-angle T- and L-shaped geometries. Two sizes (less than 10 nm) of nanorods with the aspect ratio l/d of 3.5 and 6.5 are chosen in which the spectra of longitudinal and transverse modes are fully separated and can be individually characterized. The gap distances are set in the subnanometer ($\leq$2 nm) where electron tunneling can induce charger transfer between two nanorods. For all of the nanorod dimers at D = 20 Å, we observe a redshift relative to a single nanorod for the CTP2 mode which originates from the hybridization between the longitudinal dipolar modes in end-to-end and L-shaped, transversal dipolar modes in side-to-side and transversal and longitudinal dipolar modes in the T-shaped geometry, because of the electrostatic attraction. For a smaller gap distance, the electron tunneling effect plays an important role, and, as a result, a new CTP1 mode appears and becomes stronger with the reducing gap. More importantly, we observe a large electric field enhance-

https://doi.org/10.1021/acs.jpcc.2c00105
J. Phys. Chem. C 2022, 126, 5046−5054

ment (hot spots) of the CTP1 mode in the T-shaped dimer, which distributes symmetrically surrounding the gap. Such field enhancement stems from that the electron tunneling effect at the gap increases the spill-out of electrons on the surface of the nanorod at the transverse dipolar mode. The electric field increases with decreasing gap distance and/or increasing aspect ratio. For the CTP2 mode, there is a strong electric field enhancement in the end-to-end dimer of $l/d = 6.5$ at $D = 10$ Å, which is localized in the gap and nanorod ends. The electric field increases as the aspect ratio and gap distance increase. We also find that the side-to-side dimer with a larger aspect ratio and smaller gap distance will exhibit similar plasmon resonances as a single nanorod.

AUTHOR INFORMATION

Corresponding Authors

Hongping Xiang − *School of Materials Science and Engineering, Tongji University, Shanghai 201804, P. R. China;* orcid.org/0000-0001-7255-5994; Email: xianghp@tongji.edu.cn

Lin Xu − *Biomaterials R&D Center, Zhuhai Institute of Advanced Technology, Chinese Academy of Sciences, Zhuhai 519003, China*; Email: linxu19802022@163.com

Xu Zhang − *Department of Physics and Astronomy, California State University Northridge, Northridge, California 91330-8268, United States;* orcid.org/0000-0002-6491-3234; Email: xu.zhang@csun.edu

Authors

Jiaxing Zu − *School of Materials Science and Engineering, Tongji University, Shanghai 201804, P. R. China*

Hongwei Jiang − *National Institute of Shenzhen Advanced Medical Devices Co. LTD, Shenzhen 518110, P. R. China*

Gang Lu − *Department of Physics and Astronomy, California State University Northridge, Northridge, California 91330-8268, United States;* orcid.org/0000-0002-9168-8968

Complete contact information is available at: https://pubs.acs.org/10.1021/acs.jpcc.2c00105

Notes

The authors declare no competing financial interest.

ACKNOWLEDGMENTS

This work was supported by the National Natural Science Foundation of China (51601187 and 51971159). The work at California State University Northridge was supported by the US National Science Foundation (DMR-1828019).

REFERENCES

(1) Juvé, V.; Cardinal, M. F.; Lombardi, A.; Crut, A.; Maioli, P.; Pérez-Juste, J.; Liz-Marzán, L. M.; Del Fatti, N.; Vallée, F. Size-dependent surface plasmon resonance broadening in nonspherical nanoparticles: single gold nanorods. *Nano Lett.* **2013**, *13*, 2234−2240.

(2) Habteyes, T. G. Direct near-field observation of orientation-dependent optical response of gold nanorods. *J. Phys. Chem. C* **2014**, *118*, 9119−9127.

(3) Morita-Imura, C.; Kobayashi, T.; Imura, Y.; Kawai, T.; Shindo, H. pH-induced recovery and redispersion of shape-controlled gold nanorods for nanocatalysis. *RSC Adv.* **2015**, *5*, 75889−75894.

(4) Recio, F. J.; Zabala, N.; Rivacoba, A.; Crespo, P.; Ayuela, A.; Echenique, P. M.; Hernando, A. Optical resonances of colloidal gold nanorods: from seeds to chemically thiolated long nanorods. *J. Phys. Chem. C* **2015**, *119*, 7856−7864.

(5) Li, Z. M.; Mao, W. Z.; Devadas, M. S.; Hartland, G. V. Absorption spectroscopy of single optically trapped gold nanorods. *Nano Lett.* **2015**, *15*, 7731−7735.

(6) Yin, D. Y.; Li, X. L.; Ma, Y. Y.; Liu, Z. Targeted cancer imaging and photothermal therapy via monosaccharide-imprinted gold nanorods. *Chem. Commun.* **2017**, *53*, 6716−6719.

(7) Xu, P. Y.; Lu, X. X.; Han, S.; Ou, W. H.; Li, Y.; Chen, S.; Xue, J. F.; Ding, Y. P.; Ni, W. H. Dispersive plasmon damping in single gold nanorods by platinum adsorbates. *Small* **2016**, *12*, 5081−5089.

(8) Nima, Z. A.; Davletshin, Y. R.; Watanabe, F.; Alghazali, K. M.; Kumaradas, J. C.; Biris, A. S. Bimetallic gold core-silver shell nanorod performance for surface enhanced Raman spectroscopy. *RSC Adv.* **2017**, *7*, 53164−53171.

(9) Kelly, K. L.; Coronado, E.; Zhao, L. L.; Schatz, G. C. The optical properties of metal nanoparticles: the influence of size, shape, and dielectric environment. *J. Phys. Chem. B* **2003**, *107*, 668−677.

(10) Ehrenreich, H.; Philipp, H. R. Optical properties of Ag and Cu. *Phys. Rev.* **1962**, *128*, 1622−1629.

(11) Nie, S. M.; Emory, S. R. Probing single molecules and single nanoparticles by surface-enhanced Raman scattering. *Science* **1997**, *275*, 1102−1106.

(12) Noguez, C. Surface plasmons on metal nanoparticles: the influence of shape and physical environment. *J. Phys. Chem. C* **2007**, *111*, 3806−3819.

(13) Zhao, J.; Pinchuk, A. O.; McMahon, J. M.; Li, S. Z.; Ausman, L. K.; Atkinson, A. L.; Schatz, G. C. Methods for describing the electromagnetic properties of silver and gold nanoparticles. *Acc. Chem. Res.* **2008**, *41*, 1710−1720.

(14) Ghosh, S. K.; Pal, T. Interparticle coupling effect on the surface plasmon resonance of gold nanoparticles: from theory to applications. *Chem. Rev.* **2007**, *107*, 4797−4862.

(15) Halas, N. J.; Lal, S.; Chang, W. S.; Link, S.; Nordlander, P. Plasmons in strongly coupled metallic nanostructures. *Chem. Rev.* **2011**, *111*, 3913−3961.

(16) Michaels, A. M.; Jiang, J.; Brus, L. Ag nanocrystal junctions as the site for surface-enhanced Raman scattering of single rhodamine 6G molecules. *J. Phys. Chem. B* **2000**, *104*, 11965−11971.

(17) Li, W. Y.; Camargo, P. H. C.; Lu, X. M.; Xia, Y. N. Dimers of silver nanospheres: facile synthesis and their use as hot spots for surface-enhanced Raman scattering. *Nano Lett.* **2009**, *9*, 485−490.

(18) Shegai, T.; Li, Z. P.; Dadosh, T.; Zhang, Z. Y.; Xu, H. X.; Haran, G. Managing light polarization via plasmon-molecule interactions within an asymmetric metal nanoparticle trimer. *Proc. Natl. Acad. Sci. U. S. A.* **2008**, *105*, 16448−16453.

(19) Camargo, P. H. C.; Rycenga, M.; Au, L.; Xia, Y. N. Isolating and probing the hot spot formed between two silver nanocubes. *Angew. Chem., Int. Ed.* **2009**, *48*, 2180−2184.

(20) Kinkhabwala, A.; Yu, Z. F.; Fan, S. H.; Avlasevich, Y.; Müllen, K.; Moerner, W. E. Large single-molecule fluorescence enhancements produced by a bowtie nanoantenna. *Nat. Photonics* **2009**, *3*, 654−657.

(21) Li, S.; Zhang, T. S.; Zhu, Z. J.; Gao, N. Y.; Xu, Q. H. Lighting up the gold nanoparticles quenched fluorescence by silver nanoparticles: a separation distance study. *RSC Adv.* **2016**, *6*, 58566−58572.

(22) Cheng, D. M.; Xu, Q. H. Separation distance dependent fluorescence enhancement of fluorescein isothiocyanate by silver nanoparticles. *Chem. Commun.* **2007**, *3*, 248−250.

(23) Zhu, Z. J.; Yuan, P. Y.; Li, S.; Garai, M.; Hong, M. H.; Xu, Q. H. Plasmon-enhanced fluorescence in coupled nanostructures and applications in DNA detection. *ACS Appl. Bio Mater.* **2018**, *1*, 118−124.

(24) Kim, S.; Jin, J.; Kim, Y. J.; Park, I. Y.; Kim, Y.; Kim, S. W. High-harmonic generation by resonant plasmon field enhancement. *Nature* **2008**, *453*, 757−760.

(25) Ueno, K.; Juodkazis, S.; Mizeikis, V.; Sasaki, K.; Misawa, H. Clusters of closely spaced gold nanoparticles as a source of two-photon photoluminescence at visible wavelengths. *Adv. Mater.* **2008**, *20*, 26−30.

(26) Kabashin, A. V.; Evans, P.; Pastkovsky, S.; Hendren, W.; Wurtz, G. A.; Atkinson, R.; Pollard, R.; Podolskiy, V. A.; Zayats, A. V. Plasmonic nanorod metamaterials for biosensing. *Nat. Mater.* **2009**, *8*, 867−871.
(27) Huang, X. H.; Neretina, S.; El-Sayed, M. A. Gold nanorods: from synthesis and properties to biological and biomedical applications. *Adv. Mater.* **2009**, *21*, 4880−4910.
(28) Comenge, J.; Fragueiro, O.; Sharkey, J.; Taylor, A.; Held, M.; Burton, N. C.; Park, B. K.; Wilm, B.; Murray, P.; Brust, M.; et al. Preventing plasmon coupling between gold nanorods improves the sensitivity of photoacoustic detection of labeled stem cells in vivo. *ACS Nano* **2016**, *10*, 7106−7116.
(29) Liu, Q. K.; Cui, Y. X.; Gardner, D.; Li, X.; He, S. L.; Smalyukh, I. I. Self-alignment of plasmonic gold nanorods in reconfigurable anisotropic fluids for tunable bulk metamaterial applications. *Nano Lett.* **2010**, *10*, 1347−1353.
(30) Kullock, R.; Hendren, W. R.; Hille, A.; Grafström, S.; Evans, P. R.; Pollard, R. J.; Atkinson, R.; Eng, L. M. Polarization conversion through collective surface plasmons in metallic nanorod arrays. *Opt. Express* **2008**, *16*, 21671−21681.
(31) Chu, K. C.; Chao, C. Y.; Chen, Y. F.; Wu, Y. C.; Chen, C. C. Electrically controlled surface plasmon resonance frequency of gold nanorods. *Appl. Phys. Lett.* **2006**, *89*, 103107.
(32) Wei, W. B.; Bai, F.; Fan, H. Y. Oriented gold nanorod arrays: self-assembly and optoelectronic applications. *Angew. Chem., Int. Ed.* **2019**, *58*, 11956−11966.
(33) Funston, A. M.; Novo, C.; Davis, T. J.; Mulvaney, P. Plasmon coupling of gold nanorods at short distances and in different geometries. *Nano Lett.* **2009**, *9*, 1651−1658.
(34) Pramod, P.; Thomas, K. G. Plasmon coupling in dimers of Au nanorods. *Adv. Mater.* **2008**, *20*, 4300−4305.
(35) González-Rubio, G.; González-Izquierdo, J.; Bañares, L.; Tardajos, G.; Rivera, A.; Altantzis, T.; Bals, S.; Peña-Rodríguez, O.; Guerrero-Martínez, A.; Liz-Marzán, L. M. Femtosecond laser-controlled tip-to-tip assembly and welding of gold nanorods. *Nano Lett.* **2015**, *15*, 8282−8288.
(36) Garai, M.; Gao, N. Y.; Xu, Q. H. Single-particle spectroscopic studies on two-photon photoluminescence of coupled Au nanorod dimers. *J. Phys. Chem. C* **2018**, *122*, 23102−23110.
(37) Slaughter, L. S.; Wu, Y. P.; Willingham, B. A.; Nordlander, P.; Link, S. Effects of symmetry breaking and conductive contact on the plasmon coupling in gold nanorod dimers. *ACS Nano* **2010**, *4*, 4657−4666.
(38) Shao, L.; Woo, K. C.; Chen, H. J.; Jin, Z.; Wang, J. F.; Lin, H. Q. Angle- and energy-resolved plasmon coupling in gold nanorod dimers. *ACS Nano* **2010**, *4*, 3053−3062.
(39) Biagioni, P.; Huang, J. S.; Hecht, B. Nanoantennas for visible and infrared radiation. *Rep. Prog. Phys.* **2012**, *75*, No. 024402.
(40) Lee, A.; Ahmed, A.; dos Santos, D. P.; Coombs, N.; Park, J. I.; Gordon, R.; Brolo, A. G.; Kumacheva, E. Side-by-side assembly of gold nanorods reduces ensemble-averaged SERS intensity. *J. Phys. Chem. C* **2012**, *116*, 5538−5545.
(41) Osberg, K. D.; Harris, N.; Ozel, T.; Ku, J. C.; Schatz, G. C.; Mirkin, C. A. Systematic study of antibonding modes in gold nanorod dimers and trimers. *Nano Lett.* **2014**, *14*, 6949−6954.
(42) Kar, A.; Thambi, V.; Paital, D.; Joshi, G.; Khatua, S. Synthesis of solution-stable end-to-end linked gold nanorod dimers via pH-dependent surface reconfiguration. *Langmuir* **2020**, *36*, 9894−9899.
(43) Kawawaki, T.; Zhang, H. Y.; Nishi, H.; Mulvaney, P.; Tatsuma, T. Potential-scanning localized plasmon sensing with single and coupled gold nanorods. *J. Phys. Chem. Lett.* **2017**, *8*, 3637−3641.
(44) Fontana, J.; Charipar, N.; Flom, S. R.; Naciri, J.; Piqué, A.; Ratna, B. Rise of the charge transfer plasmon: programmable concatenation of conductively linked gold nanorod dimers. *ACS Photonics* **2016**, *3*, 904−911.
(45) Urbieta, M.; Barbry, M.; Zhang, Y.; Koval, P.; Sánchez-Portal, D.; Zabala, N.; Aizpurua, J. Atomic-scale lightning rod effect in plasmonic picocavities: a classical view to a quantum effect. *ACS Nano* **2018**, *12*, 585−595.
(46) Savage, K. J.; Hawkeye, M. M.; Esteban, R.; Borisov, A. G.; Aizpurua, J.; Baumberg, J. J. Revealing the quantum regime in tunnelling plasmonics. *Nature* **2012**, *491*, 574−577.
(47) Scholl, J. A.; García-Etxarri, A.; Koh, A. L.; Dionne, J. A. Observation of quantum tunneling between two plasmonic nanoparticles. *Nano Lett.* **2013**, *13*, 564−569.
(48) Rossi, T. P.; Zugarramurdi, A.; Puska, M. J.; Nieminen, R. M. Quantized evolution of the plasmonic response in a stretched nanorod. *Phys. Rev. Lett.* **2015**, *115*, No. 236804.
(49) An, W.; Zhu, T.; Zhu, Q. Z. Numerical investigation of radiative properties and surface plasmon resonance of silver nanorod dimers on a substrate. *J. Quant. Spectrosc. Radiat. Transfer* **2014**, *132*, 28−35.
(50) Fitria, N.; Sujak, M.; Djuhana, D. The influence of gap spacing in localized surface plasmon resonance (LSPR) spectra of Ag nanorod-coupled with end-to-end assembly using boundary element method. *IOP Conf. Ser.: Mater. Sci. Eng.* **2020**, *763*, No. 012062.
(51) Huang, C. P.; Yin, X. G.; Kong, L. B.; Zhu, Y. Y. Interactions of nanorod particles in the strong coupling regime. *J. Phys. Chem. C* **2010**, *114*, 21123−21131.
(52) Xiang, H. P.; Zhang, X.; Neuhauser, D.; Lu, G. Size-dependent plasmonic resonances from large-scale quantum simulations. *J. Phys. Chem. Lett.* **2014**, *5*, 1163−1169.
(53) Xiang, H. P.; Zhang, M. L.; Zhang, X.; Lu, G. Understanding quantum plasmonics from time-dependent orbital-free density functional theory. *J. Phys. Chem. C* **2016**, *120*, 14330−14336.
(54) Xiang, H. P.; Wang, Z. L.; Xu, L.; Zhang, X.; Lu, G. Quantum plasmonics in nanorods: a time-dependent orbital-free density functional theory study with thousands of atoms. *J. Phys. Chem. C* **2020**, *124*, 945−951.
(55) Ceperley, D. M.; Alder, B. J. Ground state of the electron gas by a stochastic method. *Phys. Rev. Lett.* **1980**, *45*, 566−569.
(56) Neuhauser, D.; Pistinner, S.; Coomar, A.; Zhang, X.; Lu, G. Dynamic kinetic energy potential for orbital-free density functional theory. *J. Chem. Phys.* **2011**, *134*, 144101.
(57) Huang, C.; Carter, E. A. Transferable local pseudopotentials for magnesium, aluminum and silicon. *Phys. Chem. Chem. Phys.* **2008**, *10*, 7109−7120.
(58) Yabana, K.; Bertsch, G. F. Time-dependent local-density approximation in real time. *Phys. Rev. B* **1996**, *54*, 4484−4487.
(59) Prodan, E.; Radloff, C.; Halas, N. J.; Nordlander, P. A hybridization model for the plasmon response of complex nanostructures. *Science* **2003**, *302*, 419−422.
(60) Nordlander, P.; Oubre, C.; Prodan, E.; Li, K.; Stockman, M. I. Plasmon hybridization in nanoparticle dimers. *Nano Lett.* **2004**, *4*, 899−903.
(61) Willingham, B.; Brandl, D. W.; Nordlander, P. Plasmon hybridization in nanorod dimers. *Appl. Phys. B: Lasers Opt.* **2008**, *93*, 209−216.
(62) Jain, P. K.; Huang, W. Y.; El-Sayed, M. A. On the universal scaling behavior of the distance decay of plasmon coupling in metal nanoparticle pairs: a plasmon ruler equation. *Nano Lett.* **2007**, *7*, 2080−2088.
(63) Myroshnychenko, V.; Rodríguez-Fernández, J.; Pastoriza-Santos, I.; Funston, A. M.; Novo, C.; Mulvaney, P.; Liz-Marzán, L. M.; García de Abajo, F. J. Modelling the optical response of gold nanoparticles. *Chem. Soc. Rev.* **2008**, *37*, 1792−1805.

https://doi.org/10.1021/acs.jpcc.2c00105
J. Phys. Chem. C 2022, 126, 5046−5054